Chapter 3

Ultrafast Multidimensional NMR: Principles and Practice of Single-Scan Methods

Maayan Gal and Lucio Frydman

Department of Chemical Physics, Weizmann Institute of Science, 76100 Rehovot, Israel

3.1 INTRODUCTION

Time-domain experiments of the form

$$\text{Preparation} - \text{Acquisition versus } t \qquad (3.1)$$

play a central role in NMR.[1-3] The discrete digitization of the FID signals

$$S(t) = \sum_{\text{Acting } \Omega} I(\Omega) \exp(\mathrm{i}\Omega t) \exp\left(\frac{-t}{T_2}\right) \qquad (3.2)$$

arising in such experiments following a broadband excitation of the spins provides sufficient information for extracting the NMR frequencies that are being sought. These can be found from the Fourier transform of the FID with respect to time (FT_t)

$$I(F) = \sum_{\text{Digitized } t} S(t) \exp(-\mathrm{i}2\pi F t) \qquad (3.3)$$

A straightforward extension of these principles serves as the basis of 2D NMR, an experiment whose goal is to measure the joint $I(\Omega_1, \Omega_2)$ distribution correlating pairs of transition frequencies acting before and after the application of an optional mixing pulse sequence. By analogy with the 1D case in equation (3.1), this spectral distribution function is obtained by following the classical time-domain approach

$$\text{Preparation} - \text{evolution}(t_1) - \text{mixing}$$
$$- \text{acquisition}(t_2) \qquad (3.4)$$

proposed by Jeener[4] and generalized by Ernst *et al.*[5] (see Chapter 2). This approach provides, in turn, a

2D FID

$$S(t_1, t_2)$$

$$= \sum_{\text{Acting}\,\Omega_2} \left[\sum_{\text{Acting}\,\Omega_1} I(\Omega_1, \Omega_2) \exp(i\Omega_1 t_1) \exp\left(\frac{-t_1}{T_2}\right) \right]$$
$$\times \exp(i\Omega_2 t_2) \exp\left(\frac{-t_2}{T_2}\right) \quad (3.5)$$

that by suitable numerical FT processing

$$I(F_1, F_2) = \sum_{t_2} \left[\sum_{t_1} S(t_1, t_2) \exp(-i2\pi F_1 t_1) \right]$$
$$\times \exp(-i2\pi F_2 t_2) \quad (3.6)$$

yields the correlations being sought.

In spite of the formal similarity between this 2D FT procedure and its counterpart in equation (3.3), the acquisition of the $S(t_1, t_2)$ signal involves a fundamental difference from the 1D $S(t)$ FID collection: whereas in this latter case the acquisition time corresponds to a real-time physical variable, t_1 is in fact an evolution delay within a pulse sequence, whose effects need to be monitored over a series of N_1 independent scans. In other words, whereas 1D NMR is an experiment that can, in principle, be completed within a single transient, 2D acquisitions will–regardless of sensitivity considerations–demand the collection of numerous scans to sample the t_1 time domain adequately. There is, however, a special kind of n-D NMR experiment where the possibility arises of sampling a complete data set residing within a multidimensional time-domain space, within a single transient. This is in NMR imaging, MRI, where single-scan multidimensional schemes such as echo planar imaging have been known and exploited for decades.[6–8] Opening up this "ultrafast" 2D NMR opportunity are the very high speeds with which NMR imaging gradients $G = \partial B_0/\partial z$ can encode their information, coupled to the extreme efficiencies with which these gradient-derived effects can be refocused from the spins' evolution. Indeed, lying at the core of NMR imaging lies the use of deliberately imposed field gradients, imparting to spins that are spread over a range of positions $-L/2 \leq z \leq +L/2$, spatially dependent rotating-frame precession frequencies of the form $\omega_G = -\gamma G z$.[7,8] When considering G's action over an ensemble of excited spins, it follows that a gradient pulse of duration τ will imprint a spatially dependent pattern
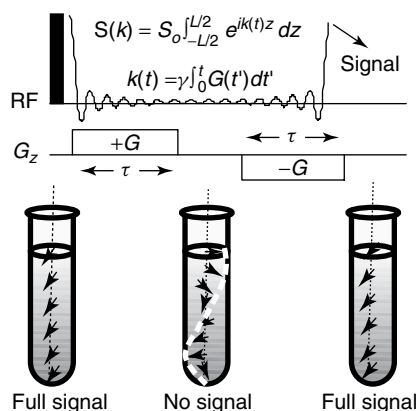

Figure 3.1. Magnetization patterns arising from the application of gradient pulses: collective destructive and constructive interference phenomena among the excited spin packets may result in observable gradient echoes.

$$M_x \xrightarrow{\gamma G z \tau} M_x \cos(\gamma G z \tau) + M_y \sin(\gamma G z \tau) \quad (3.7a)$$
$$= M_x \cos(kz) + M_y \sin(kz) \quad (3.7b)$$

defined by $k = \gamma \int_o^\tau G(t')dt'$. This wavenumber k, whose units are given in reciprocal space, describes how many turns of magnetization the gradient pulse has imparted per unit length in the sample; its value can, in principle, be made arbitrarily large–and thereby τ be made arbitrarily short–simply by working with sufficiently large G values. Because of the helical nature of the magnetization pattern in equation (3.7a), nearly null net signals will result for large k-values when the contributions arising from spins throughout a sample are summed. A reversal of the gradient coil currents, however, can rewind this pattern, leading to the regeneration of the original spin distribution and to the generation of an observable echo with nearly 100% efficiency (Figure 3.1).[a] These speed and efficiency considerations combine in echo planar imaging[6,8] to enable the sampling of complete multidimensional k-spaces–and thereby the retrieval of full NMR images–within a single scan.

Inspired by these concepts yet aware of their limitations when attempting a direct extrapolation to high-resolution NMR, we sought for ways to extend them to 2D NMR acquisitions within a purely spectroscopic context. The result of this search was

[a]Diffusion and flow are factors conspiring against this ideality but they will be disregarded throughout this study; they are treated in detail in connection to single-scan 2D NMR in Refs. 9,10.

"ultrafast NMR", an approach enabling the completion of arbitrary multidimensional NMR acquisitions within a single transient.[11-13] A key technical ingredient of ultrafast NMR, and of single-scan 2D NMR in particular, resides in translating the usual t_1-based temporal encoding process into a spatial one, whereby the internal interactions are used to create helices of spin coherences akin to those depicted in Figure 3.1. Imparting such shift-driven winding of the indirect-domain interactions required, in turn, the development of a new kind of spectroscopic manipulation; a sequence for conveying along a spatial dimension the information normally encoded by t_1, and which could be implemented within a single transient rather than through multiple scans. Reading out an observable signal from this kind of pattern also required the execution of an unusual gradient-driven acquisition stage, a process which, as mentioned, can be used to wind and unwind spin coherence patterns numerous times over the course of t_2 while monitoring the signals from the nuclei targeted. The purpose of this overview is to summarize these two main new ingredients required by ultrafast NMR–the spatial encoding of indirect-domain spectral information followed by the multiple readout of this spectroscopic information by means of an oscillatory gradient-driven process–as applied to liquid-state single-scan 2D acquisitions. Moreover, as a number of accounts describing certain aspects of these two stages have already been published,[14,15] we choose to place a special emphasis here on giving and justifying practical details that will enable potential users to execute these kinds of experiments in different commercial spectrometers.

3.2 THE BASIS OF GRADIENT-ASSISTED SINGLE-SCAN 2D NMR

As mentioned, one of the basic ingredients of single-scan 2D NMR acquisition lies in replacing the traditional temporal encoding of the indirect-domain interactions

$$M_x \xrightarrow{\Omega_1 t_1} M_x \cos(\Omega_1 t_1) + M_y \sin(\Omega_1 t_1) \qquad (3.8)$$

by an analogous spatial encoding

$$M_x \xrightarrow{t_1 \leftrightarrow Cz} M_x \cos[C\Omega_1 z] + M_y \sin[C\Omega_1 z] \qquad (3.9)$$

The indirect time-domain variable is thereby replaced by a space coordinate, according to $t_1 = Cz$, with C

a spatiotemporal parameter under our control and the z's extending over the complete sample length L.[b] The pattern in equation (3.9) represents a helix of spin magnetizations, analogous to the gradient-driven winding that was described in equation (3.7b). In general, this spatial pattern resulting from the Ω_1 spatial encoding will also lead to a null signal when averaged over the full sample; but, as in the gradient-driven winding case, its effects will be fully refocusable by the application of a reversed gradient. In contrast to the k-driven encoding arising in the imaging case, however, the spatial encoding described by equation (3.9) will be dictated by site-dependent Ω_1 interactions that are a priori unknown, and whose individual determination we are attempting. The arguments given in Figure 3.1 suggest a simple way to rapidly read out these intervening indirect-domain frequencies: if, following the encoding process given by equation (3.9), an unwinding acquisition gradient G_a is applied, the magnetization helices associated with each site in the system will undergo a shift-specific unwinding at their own site-specific instant, leading to echoes reflecting in a one-to-one fashion the $I(\Omega_1)$ NMR spectrum being sought (Figure 3.2).

It is enlightening to cast these arguments into equations: if, given a discrete $I(\Omega_1)$ spectral distribution, a spatial encoding process of the kind depicted in equation (3.9) is applied, the resulting spatially encoded signal will be proportional to

$$S_+(z) \propto [M_x(z) + iM_y(z)] \propto \sum_{\text{Acting } \Omega_1} \left[\frac{I(\Omega_1)}{L} \right]$$
$$\times \exp(iC\Omega_1 z) \exp(-Cz/T_2) \qquad (3.10)$$

The subsequent application of a common acquisition gradient G_a will then successfully read out the intervening frequencies directly from the observable macroscopic time-domain signal, according to

$$S(k) \approx \int_L dz\, S_+(z) \exp[ikz]$$
$$\approx \frac{1}{L} \sum_{\text{Acting } \Omega_1} I(\Omega_1)$$
$$\times \int_L dz[\exp(iC\Omega_1 z) \exp(-Cz/T_2)] \exp[ikz]$$
$$(3.11)$$

[b]In general, the actual encoding looks like $t_1 \leftrightarrow C(z - z_o)$ with z_o a known origin that effectively acts as a first-order phase distortion of the peaks. For simplicity and due to space constraints, we disregard this additional constant here.
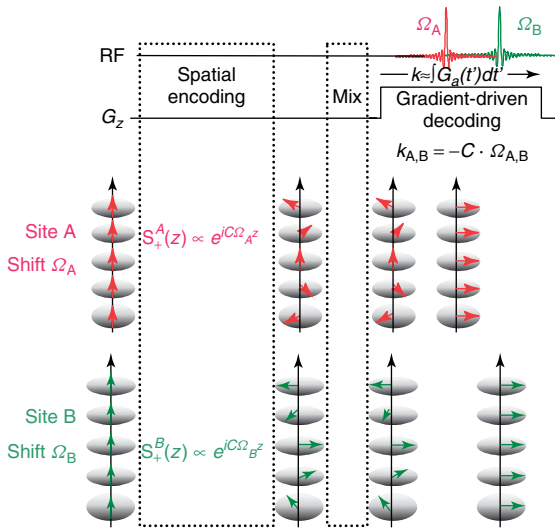
Figure 3.2. Principles of the spatial encoding and decoding approaches underlying single-scan 2D NMR, illustrated for the transverse S_+ coherences of two idealized resonances (A and B). As in Figure 3.1, windings are conferred on the sites' spin coherences; unlike those gradient-derived effects, however, these are now due to the a priori unknown interactions $\{\Omega_i\}_{i=A, B}$ that we are attempting to measure. This spatial encoding is preserved during the mixing process as either a phase or an amplitude modulation, and is read out by an acquisition gradient G_a that provides, by the positions of the corresponding observable echoes in $k = \gamma_a \int G_a(t)dt$, the associated distribution of signal intensity $I(\Omega)$.

where we have defined $k = \gamma_a \int_0^t G_a(t')dt'$. Notice that apart from a $t_1 \leftrightarrow z$ redefinition, equation (3.11) represents a Fourier analysis that is very similar to that involved in equation (3.3) or (3.6)–the only difference resting on the fact that it deals with a continuous integration carried out analogically by the G_a gradient over a $-L/2 \leq z \leq + L/2$ coordinate, rather than with a discrete FT_{t_1} summation carried out numerically on a computer over a $0 \leq t_1 \leq t_1^{max}$ interval. Aside from this technicality the overall results will be similar: a series of peaks centered at $k = -C\Omega_1$, whose shapes will be dictated by the usual T_2 effects (for an exponential decay this shape would be a Lorentzian, in the absence of decay or for a constant-time procedure it will be a *sinc* function, etc.), and whose overall integrated intensities will be proportional to $I(\Omega_1)$. In other words, the gradient-driven decoding enables a direct readout of the frequency spectrum,

acting as an FT-type computation that proceeds in an analog way and is carried out versus z (space) instead of being done digitally on a computer and versus time t_1. This, in turn, requires the k wavenumber domain to be redefined as an NMR frequency axis: the $F_1 \leftrightarrow -k/(2\pi C)$ rescaling enables a simple translation of the wavenumber values into hertz units.

Having transformed in such manner an NMR spectral determination from a temporal to a gradient-based readout process opens, in turn, the possibility of completing arbitrary 2D NMR spectroscopy determinations within a single scan. Indeed, as stressed earlier, the main features of gradient-driven echoes include the possibility of generating them very quickly and of reversing them very efficiently. A 2D NMR data set could therefore be collected by adopting the Jeener–Ernst 2D scheme in equation (3.4) and, while preserving its generality by keeping the option of using arbitrary homo- or heteronuclear *preparation* and/or *mixing* pulse sequences, modifying its encoding and decoding characteristics into

$$\text{Preparation} - \text{spatial encoding} - \text{mixing}$$
$$(t_1 \propto z)$$
$$- \begin{pmatrix} \text{gradient-driven} \\ \text{decodings/recodings} \end{pmatrix}_{N_2} \quad (3.12)$$

Notice that, in contrast to the single-gradient readout process presented in equation (3.11), data are here collected while subjecting spins to numerous decoding and re-encoding processes; specifically, to N_2 gradient oscillations $\pm G_a$ over whose course the NMR data will be continuously monitored. If properly executed each of these gradient oscillations provides the opportunity to unravel the Ω_1 indirect-domain spectrum twice: once on the $+G_a$ unwinding stage, and again during the $-G_a$ rewinding. Moreover, the times T_a over which these G_a readout gradients need to be applied can be made very short, with $T_a \leq 500\,\mu s$ durations common. As these times are much shorter than the typical T_2 decays, multiple $S(k \leftrightarrow F_1)$ indirect-domain spectra of the kind shown in Figure 3.2 can be monitored over an acquisition time $0 \leq t_2 \leq t_2^{max}$, leading to a full frequency/time-domain $S(k \leftrightarrow F_1, t_2)$ interferogram containing $2 \times N_2$ measurements of $I(\Omega_1)$ as a function of t_2. From here the full $I(F_1, F_2)$ 2D NMR spectrum being sought can then be retrieved by a 1D

FT versus the direct-domain t_2; that is, by subjecting to an FT_{t_2} each of the peaks appearing along the $S(k \leftrightarrow F_1)$ spectral domain. All this, while still requiring a single-scan acquisition for the full 2D spectral characterization.

3.3 SETTING UP A SINGLE-SCAN 2D NMR ACQUISITION

It follows from the preceding section that two unconventional procedures come into play in the acquisition of single-scan 2D NMR spectra: one is a spatially incremented evolution that makes $t_1 \propto z$; the other is the collection of signals in the presence of an oscillating gradient $\pm G_a$, resulting in an array which according to the spectrometer makes up a single-variable 1D FID(t), but which will, in fact, be processed into the desired 2D frequency spectrum $I(F_1, F_2)$. For pedagogical reasons, we have chosen to focus first on this latter, relatively straightforward processing-related procedure, leaving for later the practical aspects of how to set up the spectral window parameters and how to implement the $t_1 \leftrightarrow z$ spatial encoding (a task that actually presents a wide diversity of choices[15]).

3.3.1 Processing the Single-Scan 1D Data into a 2D Spectrum

As just mentioned, the required signal FID(t) will be collected while subjecting the spins to an oscillating gradient, which, for simplicity, we shall assume possesses a $+G_a \rightarrow -G_a \rightarrow +G_a \ldots$ square-wave shape and oscillates N_2 times with a period $2T_a$ (Figure 3.3a). The resulting 1D complex data set sampled by the spectrometer can, in fact, be viewed as being collected as a function of two independent variables: a wavenumber $k = \gamma_a \int_0^t G_a(t')dt' = \gamma_a G_a \left\{ t - 2T_a \text{int} \left[(t + T_a)/2T_a \right] \right\} (-1)^{\text{int}\lfloor (t+T_a)/2T_a \rfloor}$ that oscillates back and forth and, by doing so, reveals the full $I(F_1)$ spectrum during each interval T_a, and a direct-domain evolution time t_2, which advances monotonically for all the Ω_1 peaks in this spectrum with every $+G_a \leftrightarrow -G_a$ oscillation. It is consequently useful to cast the collected data into a
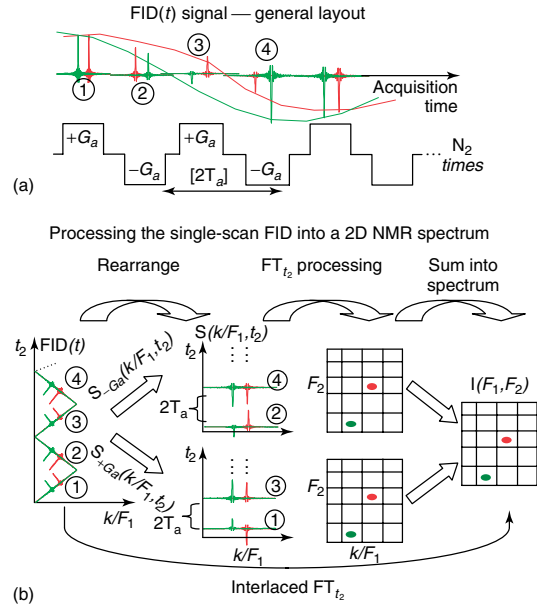

Figure 3.3. (a) Extending the single gradient-driven refocusing process illustrated in Figure 3.2, to a multiecho process capable of yielding the full $S(k \leftrightarrow F_1, t_2)$ interferogram within a single scan. In the actual experiment, the FID(t) signal arising during the course of this gradient-echo train is read out continuously. (b) Processing the single-scan FID(t) interferogram into the 2D $I(F_1, F_2)$ NMR spectrum being sought by rearranging the digitized points into two data sets, 1D FT processing along t_2, and summation of the resulting 2D spectra for signal-to-noise improvement.

function of these two variables

$$FID(t) \equiv S(k, t_2)$$

$$= \int_L dz \left\{ \sum_{\text{Acting } \Omega_2} \left[\sum_{\text{Acting } \Omega_1} I(\Omega_1, \Omega_2) \right. \right.$$

$$\times \exp(iC\Omega_1 z) \, \exp(-Cz/T_2) \Big]$$

$$\left. \times \exp(i\Omega_2 t_2) \, \exp(-t_2/T_2) \right\} \exp[ikz]$$

$$(3.13)$$

and compare the result with the traditional 2D time-domain analogs given in equations (3.5) and (3.6). One can then recognize, in this spatial integration, the result that previously arose from the numerical Fourier transformation with respect to t_1; i.e., the

bracketed sum in equation (3.6). Only an FT_{t_2} operation is thus required to obtain the desired 2D NMR spectrum from the signal $S(k \leftrightarrow F_1, t_2)$ acquired. This requires taking each complex point in turn within the 1D FID(t) array, assigning it to the correct coordinates ($k \leftrightarrow F_1, t_2$), and subjecting each $k \leftrightarrow F_1$ column in this interferogram S to full FT_{t_2} processing.

Examination of the layout imposed on the data by this 1D $\leftrightarrow$ 2D rearrangement reveals that the k points are not evenly distributed along the t_2 direction, as is required by the fast FT algorithm, because signals with different frequencies refocus at different points during the time window $2T_a$. Signals at one end of the frequency range SW_1 refocus at either end of $2T_a$, and signals at the other refocus in the middle. Two solutions exist for dealing with this inconvenience. In one of them, the $S(k \leftrightarrow F_1, t_2)$ interferogram is split into two mixed-domain data sets: an $S_{+G_a}(k \leftrightarrow F_1, t_2)$ array including all data points that were collected under the action of the $+G_a$ gradient, and an $S_{-G_a}(k \leftrightarrow F_1, t_2)$ one with all the points collected under the $-G_a$ gradient. Rows within each of these subsets appear now equispaced along t_2 for each of the sampled $k \leftrightarrow \omega_1$ points, with an increment given by $\Delta t_2 = 2T_a$ (Figure 3.3b). The fast FT algorithm can then be executed along this latter dimension to yield a pair of $I_{\pm G_a}(F_1, F_2)$ spectra and, since both of these traces contain identical spectral information, it is, in principle, possible to combine them so as to obtain a final 2D spectrum with an additional $\sqrt{2}$ enhancement in the signal-to-noise ratio (SNR). In practice, this co-addition often necessitates a prealignment of the peaks along the $k \leftrightarrow F_1$ dimension, as echo peaks in the corresponding $I_{\pm G_a}(F_1, F_2)$ spectra may be shifted along this direction by nonidealities associated with gradient-switching delays and/or time delays at the start of the data acquisition.[c] An alternative option consists of separating the data points into two sets but then processing these resulting $S_{\pm G_a}(k \leftrightarrow F_1, t_2)$ data matrices in a single, combined FT_{t_2} operation known as the *interlaced FT*.[16,17] This allows one to achieve a smaller effective $\Delta t_2 = T_a$; for given indirect- and direct-domain spectral widths SW_1 and SW_2, it can be shown that this brings about an additional $\sqrt{2}$ improvement in SNR.[18] It should be noted, however, that for this operation to succeed an even more stringent

alignment of the $+G_a$ and $-G_a$ echoes along the k axis is required, and that the actual SNR gains decrease toward the edges of the $k \leftrightarrow F_1$ range.[d]

In addition to these data rearrangement and FT_{t_2} considerations, processing the single-scan 2D data may require additional provisions that are not usual in conventional 2D NMR. The most common among these arises from the potential need to "straighten out" the data in the $S_{\pm G_a}(k \leftrightarrow F_1, t_2)$ interferograms in order to correct for imbalances between the strengths of the $+G_a$ and $-G_a$ decoding gradients (Figure 3.4). While this nonideality should preferably be removed by balancing gradients at the hardware level, this may not always be the most practical solution, as it may require repeated adjustments and be susceptible to changes over time. Alternatively, if at least one of the $k \leftrightarrow F_1$ echo peaks (e.g., the solvent's) can be clearly discerned within the interferogram, the possibility arises to compensate for these gradient imbalances by a manual interactive shearing of the data. For example, a continuous linear shearing of the 2D set can be conveniently imparted by applying a t_2-dependent phase shift $\phi(t_2) = \sigma z t_2$ of the signals in a Fourier domain that is conjugate to $k \leftrightarrow F_1$; i.e.,

$$S(k, t_2) \xrightarrow{FT_k^{-1}} S(z, t_2) \xrightarrow{\exp(iz \cdot \sigma \cdot t_2)} S(z', t_2)$$
$$\xrightarrow{FT_z} S_{\text{sheared}}(k, t_2) \tag{3.14}$$

The linear t_2 dependence assumed in this σ-shearing suffices to compensate for most common distortions, including gradient imbalances; if severe eddy current effects are present, however, more complex distortions of the echoes may arise and more complicated $\phi(t_2)$ shearing functions be needed.

In addition to the FID(t) $\rightarrow S(k \leftrightarrow F_1, t_2)$ rearrangement and to the shearing operations, other more common pre-FT manipulations may have to be carried out on the data, including baseline correction, weighting, linear prediction, and zero filling. In the t_2 domain, these "massaging" operations can be carried in the usual row-by-row fashion. Along the $k \leftrightarrow F_1$ domain, however, we find it convenient to perform all these ancillary operations (interactively if needed) on inverse Fourier transformed "z-axis" data; forward-transforming the data back along both the z and t_2 domains is then needed before the final

[c]This alignment can be carried out by appropriately left-shifting the raw *FID(t)* data prior to their subdivision and rearrangement into the two $S_{\pm G_a}(k \leftrightarrow F_1, t_2)$ subsets.

[d]All timing delays between the $+G_a \leftrightarrow -G_a$ transitions should be included in the actual computation of SW_2 and in the FT_{t_2}-interlacing process, including gradient-switching times and heteronuclear decoupling pulses if present (vide infra).
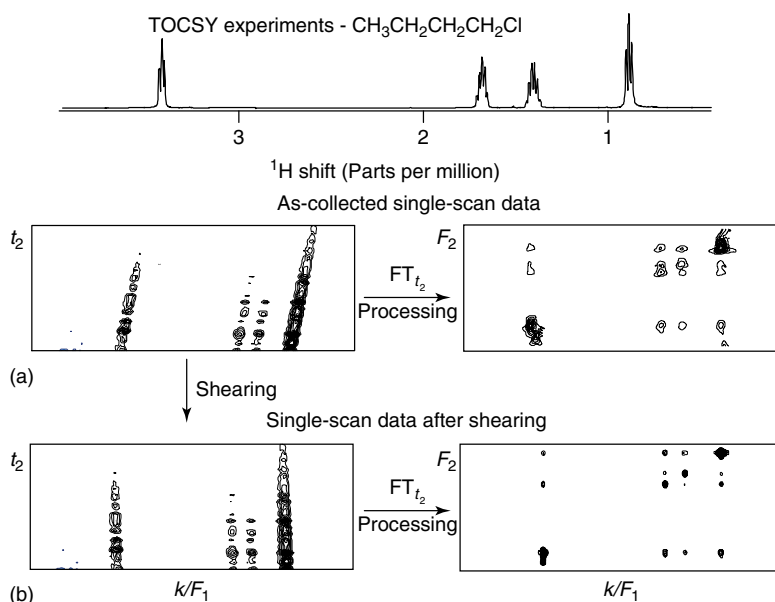
Figure 3.4. Shearing problems arising in single-scan 2D NMR even from minor (<0.1%) gradient imbalances, illustrating their ensuing spectral consequences and their postacquisition software-based correction for the ultrafast TOCSY spectrum of *n*-butyl chloride.

phase/magnitude calculation and the plotting of the spectra.

3.3.2 Setting Up the Single-Scan 2D NMR Spectral Windows

Considerable differences between the indirect and direct domains arise among the parameters that define the widths, resolutions, and offsets that determine the spectral windows of single-scan 2D NMR experiments. Spectral width and resolution considerations are exactly as in conventional FT NMR for the F_2, direct, domain: the spectral window SW_2 is given by the inverse sampling rate $(\Delta t_2)^{-1}$, i.e., by $(2T_a)^{-1}$ if using a conventional two-set FT_{t_2} or by $(T_a)^{-1}$ if relying on a single-set interlaced FT_{t_2}. Spectral resolution will also be as usual in this domain, determined by the inverse of the overall acquisition time: $\Delta F_2 = (\pi t_2^{max})^{-1}$. Along the indirect F_1 domain, in contrast, the accessible spectral window will depend on the range of wavenumbers $k_{max} = \gamma_a \int_o^{T_a} G_a(t')dt'$ explored by the $\pm G_a$ acquisition gradients during their acting times T_a. Assuming for simplicity that these gradients have

a square-wave shape (often a good assumption in high-resolution systems), the resulting spectral width becomes $SW_1 = \gamma_a G_a T_a/2\pi C$; since T_a also defines SW_2, minimizing this latter window or relying on an interlaced FT_{t_2} allows one to reduce the gradient demands and thereby relax the experimental demands. Notice the central role that the spatiotemporal parameter C, which, as mentioned, relates position to indirect-domain evolution according to $t_1 = Cz$, plays in defining the spectrum. Assuming that one employs the full available sample length $-L/2 \le z \le +L/2$ (dictated by the RF coil's geometry and typically spanning 16–18 mm in 5 mm NMR probes) to carry out the experiment, then the sole variable controlling C becomes t_1^{max} – the equivalent of the overall t_1 evolution time. In general, and for reasons akin to those arising in conventional 2D spectroscopy, it can be shown that experiments relying on constant-time encoding modes lead to a more efficient spatiotemporal factor $C = 2t_1^{max}/L$, whereas real-time experiments result in a smaller coefficient $C = t_1^{max}/L$.[e] C will also be involved in defining

---

[e]Then, as example, a real-time encoding employing a conventional two-set FT_{t_2} will have a gradient-controlled indirect-domain window $SW_1 = \frac{\gamma_a G_a L/(2\pi)}{2t_1^{max} SW_2}$.

the spectral resolution ΔF_1 that an experiment will have in the indirect domain. Indeed, it follows upon applying the uncertainty relations to the analog FT_k in equation (3.11) that the closest wavenumber separation Δk that the gradient-driven unwinding will be able to resolve is L^{-1}–corresponding to a single-turn difference between two sites when considered over the full sample. In terms of spectral resolution, this translates into $\Delta F_1 \approx \Delta k/2\pi C = 1/t_1^{\max}$, just as in conventional 2D NMR acquisitions.[3]

As for the carrier offsets characterizing the 2D spectral frame, these will once again be affected by different considerations depending on whether one discusses the direct or the indirect domain. In either of the FT_{t_2} processing modalities discussed above quadrature detection will be available along F_2, and a central offset suitable for all peaks can be chosen for this domain in a conventional, 1D-like fashion.[f] Detection along the F_1 domain, on the other hand, will be carried out in phase-sensitive fashion by the G_a-driven decoding, which will start reading out the spectrum at one end and progress steadily toward the other.[g]

The actual distribution of "peaks" through this sweep will depend on whether the initial spatial encoding was carried out using an $\exp[iC\Omega_1 z]$ phase modulation, leading to a single set of echoes at $k = -C\Omega_1$, or using a $\genfrac{}{}{0pt}{}{\cos}{\sin}[C\Omega_1 z]$ amplitude modulation, involving the effective winding of two opposing magnetization helices, and leading to mirror-image peaks at $k = -C\Omega_1$ and $k = +C\Omega_1$. The latter is the most common kind of modulation in 2D NMR and, given its loss of information on the sign of Ω_1, it requires the spatial decoding to be carried out in an asymmetric, off-center manner. This, in turn, can be achieved in two different fashions: one involves shifting the carrier of the RF pulses employed to impart the spatial encoding away from the center of the F_1 axis by an offset $SW_1/2$; the other involves working on-resonance but applying at some point during the course of the RF-free t_1 evolution, an extra gradient pulse generating a winding $k_{\text{shift}}/2\pi =$

$\gamma_e G_{\text{shift}}\tau_{\text{shift}}/2\pi = CSW_1/2$. This is distantly akin to a coherence-selection gradient pulse, and will effectively shift all the peaks of interest by half a spectral width. It is also convenient to precede the k/t_2 read-out acquisition by a purging short gradient pulse (in the order of $10\,\text{cm}^{-1}$) so as to fully dephase any residual magnetization that may have remained unencoded after the mixing. The resulting echo time shift k_{purge}/C will also affect the peak positions in the indirect domain, and should also be accounted for as described above when setting the desired limits of the F_1 spectral window. Illustrations of how these various parameters affect single-scan 2D experiments, and of how to set them up, are given in the next section.

Two final parameters worth highlighting in connection with single-scan 2D NMR acquisitions are the actual physical dwell times Δt and the filter bandwidths (fb) that should be used throughout the physical data sampling process. In conventional acquisitions, these two parameters are governed by the characteristics chosen for the direct-domain frequency axis, according to $SW_2 = (\Delta t)^{-1} \approx 2fb$, and fb is usually of the order of few kilohertz. In single-scan 2D NMR, by contrast, we saw that SW_2 is related to T_a and that within each of these intervals *all* of the $k \leftrightarrow F_1$ points in the final interferogram need to be digitized. It turns out that whether derived by ΔF_1 resolution or by maximum bandwidth considerations, Δt and fb are again related in the single-scan 2D case by $(\Delta t)^{-1} \approx 2fb$; but this time $2fb$ will be given by $\gamma_a G_a L/(2\pi)$, which is the total range of resonance offsets within the sample. Setting fb accordingly minimizes the incoming noise without affecting the ΔF_1 resolution: smaller values compromise the latter (resulting in a shorter effective sample) while bigger ones incur an extra SNR penalty. At the same time, if the spectrometer allows filtering and sampling characteristics to be chosen independently, oversampling the 1D FID(t) at dwell times Δt smaller than $2\pi(\gamma_a G_a L)^{-1}$ is convenient, as this ensures that digitization issues do not end up defining any of the spectral characteristics. Opening up the filter bandwidth to accommodate a $\gamma_a G_a L/2\pi$ range whose value is often in the tens of kilohertz implies that, although on a per-scan basis the ultrafast 2D NMR signal will ideally be identical to that in conventional NMR, the noise will be substantially larger. Indeed for identical SW_1, ΔF_1, and SW_2 requirements, it can be shown that the ratio between the noise level in conventional and in ultrafast 2D experiments will be given by $fb^{\text{ultrafast}}/fb^{\text{conventional}} \approx \frac{\gamma_a G_a L/2\pi}{(\Delta t_2)^{-1}} = SW_1 t_1^{\max}$; in

---

[f]Still, minimizing G_a's amplitude and thereby maximizing SNR suggests working with the minimum possible SW_2. This, in turn, calls for centering the carrier's acquisition frequency exactly in the middle of the spectrum to be observed, rather than, for instance, on resonance with the H_2O peak as is common in biomolecular NMR experiments.

[g]This analog decoding is akin to a continuous-wave type sweep and will therefore be free from the folding phenomena common in FT NMR, unless the spatial encoding is done using discrete, frequency-stepped RF pulses.[12]

Table 3.1. Relations between various spectral parameters in ultrafast 2D NMR[a]

Fixed experimental parameters (define first)	Parameters to be set at a desired value		Physical parameters to be adjusted		Additional comments/ operations to be carried out
γ_e, γ_a: excitation and acquisition magnetogyric ratios	SW_2: direct-domain spectral width	⇒	Set $T_a = \frac{0.5}{SW_2}$ (or $\frac{1}{SW_2}$ if interlaced FT used)	⇒	Round T_a off to an integer multiple of the physical time Δt, and recalculate the actual SW_2 based on this exact time value plus whatever gradient-switching and/or decoupling pulse delays δ may have been used.[c]
L: effective sample (coil) length	Δv_2: direct-domain spectral resolution	⇒	Set number of acquisition loops $N_2 = \frac{SW_2}{\Delta F_2}$	⇒	N_2, T_a, and Δt define in turn the total number of complex points to be digitized in the scan.[d]
Δt: physical dwell time to be used in (over)sampling each FID(t) complex point	Δv_1: indirect-domain spectral resolution	⇒	Set overall encoding time $t_1^{max} \approx \frac{1}{\Delta F_1}$.[e]	⇒	Defines in turn the important spatiotemporal parameter C; $C \approx \left\{ \begin{array}{c} \frac{t_1^{max}}{L} \\ \frac{2t_1^{max}}{L} \end{array} \right\}$ for $\left\{ \begin{array}{c} \text{real-} \\ \text{constant-} \end{array} \right\}$ time encoding modes
G_e: encoding gradient[b]	SW_1: indirect-domain spectral width	⇒	Set acquisition gradient $G_a = \frac{SW_1 \cdot C}{\gamma_a T_a}$	⇒	G_a also defines the optimum filter bandwidth required for maximizing SNR: $fb \approx \left\{ \pm \frac{\gamma_a G_a L}{4\pi} \right\}$ (regardless of Δt)
	O_2: direct-domain central offset	⇒	Set as in conventional 1D NMR	⇒	It is often convenient to use optimized excitation/acquisition offsets so as to minimize SW_2
	O_1: indirect-domain central offset	⇒	Set away from desired center of dimension by $\frac{SW_1}{2}$	⇒	Can be carried out by applying the spatial encoding chirp pulses using a carrier that is $\pm \frac{SW_1}{2}$ away from the center of the spectrum, or by inserting a "shifting" gradient pulse $k_{shift} \approx \pm \frac{SW_1}{4\pi C}$ in between the encoding pulses[f]

[a]Refer to Figure 3.5 for further definitions of the different parameters
[b]To be set to $\approx \frac{10 \cdot SW_1}{\gamma_e L}$
[c]For instance in the normal FT case this would mean recalculating $SW_2 = \frac{1}{2(T_a + \delta)}$
[d]Number of complex points $= \frac{2N_2 T_a}{\Delta t}$ if using explicit acquisitions during T_a, or $= \frac{2N_2(\delta + T_a)}{\Delta t}$ if using a regular digitization starting at $t_2 = 0$
[e]In actuality the indirect-domain half-widths end up $\approx$50% wider than expected; see Refs. 15,19 for further discussions on purely absorptive versus mixed-phase lineshapes
[f]An additional offset shift $2\pi \Delta O_1 \approx \frac{k_{purge}}{C}$ should be included to account for the short k_{purge} gradient pulse used to clean up residuals prior to the direct-domain acquisition

other words, by the number of sample points characterizing the indirect domain. All other things being equal (including, in addition to the parameters just mentioned, the overall number of t_2 points, relaxation decays, etc.) the per-scan SNR in single-scan 2D NMR experiments will therefore be poorer than in conventional counterparts by ca. the square root of this factor.

It follows from all these arguments that, in addition to certain fixed parameters such as the sample length L, magnetogyric ratios, etc., a number of independent and interrelated variables are involved when setting up a single-scan 2D NMR experiment. Table 3.1 summarizes one possible way to treat these variables in an integrated fashion when setting up the spectral windows of 2D acquisitions.

3.4 SETTING UP SINGLE-SCAN 2D NMR's SPATIAL ENCODING

As mentioned in 3.2, a defining stage of single-scan 2D NMR acquisition consists of imposing a shift-driven spatial encoding of the spin interactions, i.e., of making the indirect-domain evolution time proportional to a spin's position. Many different strategies have been proposed and demonstrated for imposing such a $t_1 \alpha z$ connection; all of these rely on the combined application of an encoding field gradient G_e that, acting in unison with frequency-selective RF pulse sequences, addresses incremented positions at incremented times by a sequential excitation, inversion, or storage of the spin coherences.[20–26] Common to all these manipulations are a frequency-incremented RF irradiation and a refocused gradient G_e that yield, at their conclusion, a spatial winding of the magnetization that encodes spectroscopic information according to $\Omega_1 z$. A comprehensive review of many of these methods, including both an explanation of their physical principles as well as their mathematical basis, has been given recently[15] and will therefore not be repeated here. This section is devoted instead on describing how to set up two closely related encoding modes, one imparting a real-time spatial imprint and the other a constant-time evolution, for basic homo- and heteronuclear 2D correlation sequences in two common kinds of commercial instruments.

Figure 3.5 illustrates the two encoding modes that will be addressed here. Unlike the stepwise Δt_1 incrementation used in conventional 2D NMR,

both these approaches rely on a continuous manipulation of the physical variable z for monitoring the indirect-domain evolution. The real-time amplitude-modulated scheme in Figure 3.5(a) begins and concludes the t_1 period with a pair of chirped $\pi/2$ pulses acting during the course of a $+G_e/-G_e$ gradient waveform;[20] the constant-time phase-modulated scheme in Figure 3.5(b) also includes a pair of chirped pulses acting during the course of a bipolar gradient, but this time their amplitudes are set to cause π inversions and are therefore preceded by an initial $\pi/2$ pulse to trigger the excitation of the spin coherences.[24] The two $\pi/2$ pulses in the first of these sequences will first excite and then store the spin coherences sequentially from one end of the sample to the other, endowing spins at one extreme with an effective evolution time $t_1 = 0$ and those at the other extreme with $t_1 = t_1^{max}$. The two π pulses in the second sequence will refocus the indirect evolution progressively from one sample extreme to the other, leading to an effective t_1 evolution of $-t_1^{max}$ at one end of the sample, of ≈ 0 at the center, and of $+t_1^{max}$ at the other extreme. Notice that both sequences rely on bipolar $\pm G_e$ gradient waveforms, a procedure meant to refocus the effects imparted by the gradient and leave only spectroscopic information at its conclusion.

It is possible to rationalize either of the swept schemes illustrated in Figure 3.5 by considering that spins at specific positions z will only be affected when the RF's time-dependent offset, $O(t)$, matches their resonance frequency according to

$$\Omega_1 \pm \gamma_e G_e z = O(t_1) \qquad (3.15)$$

where the $\pm$ sign accounts for the polarity reversal in G_e's waveform. It follows that to ensure a t_1 evolution that varies linearly with z as required by the ultrafast scheme, the offset $O(t)$ needs to be swept linearly in time according to $O(t) = O_i + Rt$, with O_i as an initial frequency value and R as the offset sweep rate. Triggering, storing or refocusing the Ω_1 effects in this fashion brings about the desired $\phi_1 \propto C\Omega_1 z$ form of encoding. It is also convenient to assume that each of these RF sweeps, lasting a time $\tau_{RF} \approx t_1^{max}/2$ each, covers the same symmetric range $2\pi O_i = -\gamma_e G_e L/2 \rightarrow 2\pi O_f = +\gamma_e G_e L/2$. The Ω_1 effects thus encoded will include an off-resonance value, which will be defined in the usual NMR fashion according to the spectrometer's main carrier offset at the time of the chirping. As the overall encoding will proceed over a time t_1^{max} and encompass an overall sample length
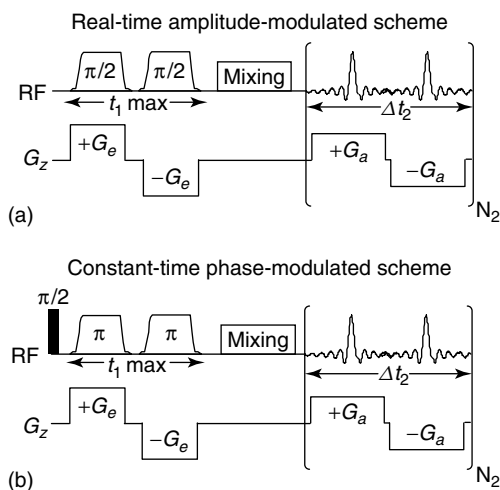
Figure 3.5. Combined gradient/RF manipulations underlying the continuous real-time (a) and constant-time (b) versions of the spatial encoding treated in this study, assuming for simplicity 2D homonuclear correlations. In both cases, two identical RF pulses are applied, sweeping between initial and final offsets $\pm\gamma_e G_e L/2$ at rates $2\pi R = \pm 2\gamma_e G_e L/t_1^{max}$ with amplitudes set so as to impart net $\pi/2$ or π rotations of the spins at all positions.

L, C therefore has the value $\frac{t_1^{max}}{L}$ for the real-time sequence and $\frac{2t_1^{max}}{L}$ for the constant-time one. As for programming these swept pulses, this is most conveniently done in modern spectrometers by modulating the outgoing RF with two table-stored waveforms: one containing the phase and the other the amplitude modulation to be imparted to an otherwise constant pulse within a constant rotating frame. The values to be stored in the phase-table should be computed according to

$$\phi_{RF}(\tau) = \int_0^\tau [O_i + Rt']dt' = \gamma_e G_e L\tau \left(\frac{\tau}{t_1^{max}} - \frac{1}{2}\right)$$
$$\tau = 0, \Delta\tau, \ldots, N_i \Delta\tau = \frac{t_1^{max}}{2}. \qquad (3.16)$$

This table's clocking-out dwell time $\Delta\tau$ needs to be chosen sufficiently small to fulfill the Nyquist criterion associated with a sweep of full bandwidth $\gamma_e G_e L$, i.e., $\Delta\tau \leqslant \frac{2\pi}{2\gamma_e G_e L}$, while remaining compatible with the spectrometer's waveform storage capabilities. As for the amplitudes to be given to the chirped pulses, these will, in turn, depend on whether the swept RF pulses will be imparting $\pi/2$ spin

excitations/storages, or π rotations. In either case it can be shown, both numerically and by analytical derivation,[20,27,28] that the ensuing RF field amplitudes will have to be adjusted in proportion to the square root of the rate $R \approx \frac{(\gamma_e G_e L/2\pi)}{(t_1^{max}/2)}$ at which the RF sweeps through the targeted range. Specifically, $\gamma B_1 \approx 0.25\sqrt{|R|}$ (all in kilohertz) will induce progressive $\pi/2$ nutations of the spins, while setting γB_1 to ≈ 2.2 times this value will generate an adiabatic-like π refocusing of the spins being swept.[h] Notice that among all these indications on how to set up the spatial encoding process, no constraint arises on what G_e value should be used. It turns out that this variable does not end up defining, for either of these continuous spatial encoding sequences, either the spectral window or the encoding characteristics of the experiment. It can be shown, however, that increasing G_e's value will bring about progressive diffusion-related SNR losses,[9,10] while decreasing it below $\approx \frac{40}{\gamma_e L t_1^{max}}$ and/or $\approx \frac{10SW_1}{\gamma_e L}$ will violate the assumption given in equation (3.15) and thereby also impair the SNR and quality of the $k \leftrightarrow F_1$ peaks. It is therefore convenient to work with the lowest possible value of $\gamma_e G_e$ that remains compatible with these latter conditions.

While computer scripts can be written to generate the amplitude- and the phase-modulating waveforms that are needed to create these spatially encoding $\pi/2$ or π RF pulses, all major manufacturers of NMR (and MRI) hardware provide, as part of their spectrometer-controlling software, the tools to do so within the environment of their operating systems—either by using commands, set-up macros, or within the pulse sequence programming codes themselves. Table 3.2 summarizes, for two common kinds of instrument, possible ways of generating the associated waveforming tables. Matlab® scripts capable of generating these tables can also be provided upon request. For completeness, we also present in Table 3.3, for the two types of spectrometer, routes by which data points in single-scan 2D NMR can be collected in the presence of oscillating gradient waveforms.

---

[h]While the fact that R is constant implies that fixed-amplitude tables could be used for programming these pulses' envelopes, it is customary to smooth the beginning and end of these sweeps with a rapidly decaying WURST-type function.[29]

Table 3.2. Setting up frequency-swept excitation/inversion spatial encoding pulses in Varian and Bruker spectrometers[a]

Input (known) parameters	Pulse generation procedure – Varian	Pulse generation procedure–Bruker
Pulse bandwidth $pbw = \gamma_e G_e L/2\pi$	***Input:*** Use the *Pbox* command '*Pbox chirp.RF – w wurst pbw/pdur -s 1.0 – p p90lvl – l p90*',	***Input:*** Type *stdisp* in the command line, which opens the graphical shaping interface.
Pulse duration $pdur = \frac{t_1^{max}}{2}$	which assumes a 1 µs dwell and a WURST-type envelope based on a wavelib file giving a π/2 nutation if its adiabaticity factor is set to 0.44, and a π nutation if set to 4.0	Choosing then through the menus: *shapes* → *adiabatic shapes* → *wurst* or *smoothed chirp* opens a window where a default table length (1000) is given, and *pdur* and *pbw* (total sweep width) are inserted. After saving the pulse with a desired name, (e.g., *userchirp*) choose through the menus *analysis* → *integrate adiabatic shape* and insert the *pdur* and *p90* reference values
Hard π/2 duration *p90*		
Hard π/2 RF power level *p90lvl*	***Output****: the *Chirp.RF* file containing the pulse to be digitized and the *chirp_pwr* RF gain to be used.	***Output:*** The *userchirp* file containing the pulse and, from *p90lvl*, the power differential by which the swept pulse should be attenuated (if inputting *p90lvl* but employing a π sweep, decrease this *stdisp* differential by 6 dB)
	Operational example: *obspower(chirp_pwr)* *shaped_pulse("chirp",pdur,v1,rof1,rof1)*	***Operational example:*** *(5u p11: sp11 ph0):f3* with *p11 = pdur*, *spnam11 = 'userchirp'* and *sp11* set as the RF power differential plus *p90lvl*

[a]For example only; actual implementation and operation may vary from system to system. Refer to the text for further definitions of the different parameters, and to the manufacturer's manual for technical assistance

3.5 SINGLE-SCAN 2D NMR: WORKED EXAMPLES

We conclude this description with a number of examples of the ultrafast 2D NMR methodology; this section, in particular, presents worked-out descriptions of a single-scan real-time-encoded 2D homonuclear acquisition on a Varian 500 MHz NMR machine, and of a constant-time 2D heteronuclear experiment on a Bruker 800 spectrometer. Each example highlights the effects of the various parameters introduced in the preceding section.

Table 3.3. Setting up single-scan 2D data acquisitions under the action of gradients for Varian and Bruker spectrometers[a]

Input (known) parameters	Explicit acquisition procedure – Varian[b]	Implicit acquisition procedure – Bruker[c]
Number of acquisition loops $N2$	*Preparation:* Use the input parameters to set $np1 = 2T_a/\Delta t$ (# of total points sampled per T_a) and $acqdel = \Delta t$	*Preparation:* Use the input parameters to set $gp3 = -gp4 = G_a$ (in % values), $p16 = T_a$, $td = 2 \cdot \# \ points$, $l4 = N2$,
Loop duration T_a		
	Execution:	*Execution:*
Acquisition gradient G_a	```rcvron();``` ```Initval(N2, vx);``` ```starthardloop(vx);``` ```shapedgradient(''gsquare'', Ta,Ga,'z',1,NOWAIT);```	```DE1 DE2 DERX DEADC DEPA``` ```7 p16:gp3``` ``` D7``` ``` (p7 ph0):f3```
Total number of complex digitized points # points	```acquire(np1,acqdel);/* explicit acquisition */``` ```Rcvroff(); xmtron();``` ```Xmtroff(); rcvron();``` ```delay(5u);``` ```shapedgradient(''gsquare'', Ta,-Ga,'z',1,NOWAIT);```	``` D7``` ``` p16:gp4``` ``` D7``` ``` (p7 ph0):f3``` ``` D7``` ``` lo to 7 times l4```
Effective (over)sampling dwell time Δt per complex point	```acquire(np1,acqdel);/* explicit acquisition */``` ```rgradient('z', 0.0);``` ```Rcvroff(); xmtron();``` ```Xmtroff(); rcvron();``` ```delay(5u);``` ```endhardloop();```	

[a]For example only; actual implementation and operation may vary from system to system
[b]Assuming a homonuclear experiment with no decoupling (e.g., Figure 3.6)
[c]Assuming a heteronuclear experiment with ^{1}H acquisition and X decoupling by π pulses on third channel (e.g., Figure 3.7)

The first of the exemplified pulse sequences (Figure 3.6a) involves a TOCSY version incorporating a pair of $\pi/2$ chirped pulses for the spatial encoding, a ca. 60 ms long transverse isotropic mixing period, a short purging gradient pulse to clean up residual signals after the recall of the amplitude-modulated magnetization, and a square-wave oscillating acquisition gradient incorporating a short gradient recovery delay. Fixed parameters for this experiment included 1 ppm $\equiv$ 501 Hz, $L = 1.8$ cm, and a physical oversampling dwell time Δt set to 2 µs ($SW = 500$ kHz). The targeted sample, *n*-butyl chloride, exhibits resonances between 0.9 and 3.2 ppm; on the basis of this, spectral windows $SW_1 = SW_2 = 2200$ Hz were chosen. Since a conventional FT_{t_2} was going to be used for processing the resulting data, the chosen SW_2 value plus the gradient recovery time (10 µs) led to a $T_a = \frac{1}{2 \times 2200} - 10^{-5}$ s. This number was then rounded to 226 µs so as to allow for accommodating an integer number of digitized data points, and the carrier offset along ν_2 was centered at the center of the spectrum (*tof* $= -1405$ Hz from the usual 5 ppm reference). In terms of spectral resolution, we chose $t_1^{max} = 30$ ms, which in turn set the duration of the $\pi/2$ chirped pulses to 15 ms. With the t_1^{max} and T_a values thus defined, the G_a needed in order to accommodate the desired SW_1 also
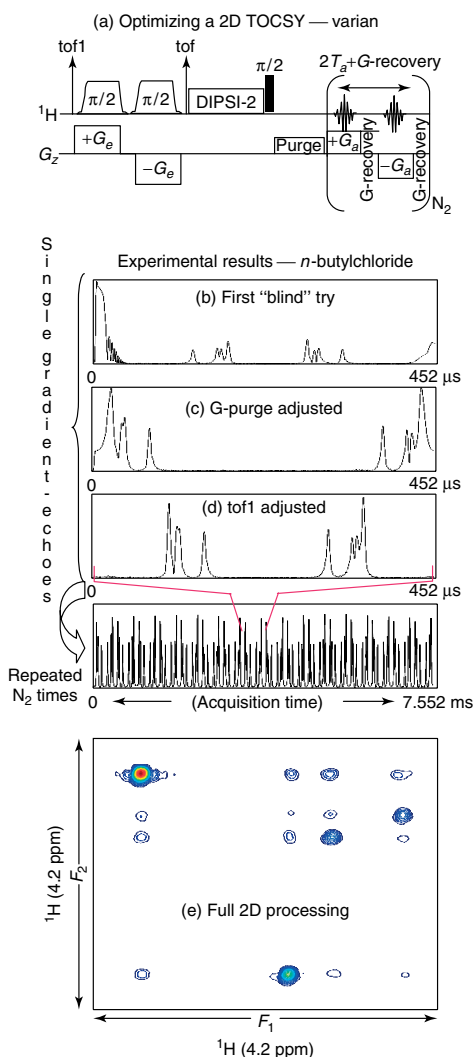
Figure 3.6. (a) Sequence of events involved in the optimization of a single-scan 2D NMR acquisition, illustrated with a ^{1}H TOCSY acquisition on *n*-butyl chloride executed on the basis of an amplitude-modulated spatial encoding sequence on a Varian spectrometer. The parameters summarized in Table 3.1 lead to the gradient-echo pattern shown in (b), encompassing the four echoes being sought as well as spurious signals arising from unencoded magnetization. A small gradient purge pulse (20 G cm^{-1} for 100 μs) cleans this up (c), but does not use the available $k \leftrightarrow F_1$ window optimally; this can be corrected by a minor adjustment of the *tof1* offset value used for the chirped encoding (d). Repeating this gradient echo numerous times N_2 leads to the full *FID(t)* signal, which by processing results in the final spectrum sought (e).

follows: $G_a = 2\pi \frac{SW_1 t_1^{max}}{\gamma_a L T_a} = 38.1$ G cm^{-1}; this in turn led to setting $fb = \gamma_e G_a L/(4\pi) = 145$ kHz for the analog acquisition filters. t_2^{max} was chosen to be 7.4 ms. Dividing this by $2T_a$ set the number of $\pm G_a$ acquisition loops to be used to $N_2 = 16$–leading to an actual $t_2^{max} = 7.552$ ms when considering the T_a and gradient-switching time values, as well as to an overall number $np = 7232$ of real plus imaginary points collected ($np = 4T_a N_2 SW$). As for the choice of encoding gradient, this is, as mentioned, flexible; relying on the condition $\gamma_e G_e L \geq 10 SW_1$ suggested making $G_e \approx 15$ G cm^{-1}, which is a reasonable value for homonuclear experiments. This defined the final parameter needed to compute the frequency-chirped pulses (*pbw*, cf. Table 3.2); these two identical waveforms were computed as defined in Table 3.2 and their common offset was set off-center by $\approx SW_1/2$ in the ω_1 domain (i.e., *tof1* $= -4300$), in order to account for the nonquadrature detection and the effect of the final purging pulse.

Although setting up single-scan 2D sequence parameters proceeds relatively straightforwardly according to these recipes (all that was needed was the center offsets and choices of the spectral widths and resolutions along both axes), the procedure may still require a certain degree of fine tuning in order to reach an optimum data set. This optimization will mostly focus on centering the echoes arising in the $k \leftrightarrow F_1$ dimension so as to suit the chosen $SW_{1,2}$ windows, and it can be easily checked by examining the echo dispositions arising in the first t_2 point of the 2D interferogram. For instance, inspection of the data arising for the above-mentioned parameters (Figure 3.6b) reveals that this first trace is still not perfect: all four chemical sites in the molecule can be discerned as individual echoes, but there is still a residual signal at the beginning of the acquisition arising from magnetization that did not undergo encoding,[i] as well as a slight shift in the echoes from the center of the SW_1 window. Increasing the purging pulse amplitude and concomitantly changing the offset *tof1* of the chirped pulses can take care of these deficiencies (Figure 3.6c and d); once this is satisfactorily resolved, the various processing steps detailed

[i]Residual nonencoded magnetization can be distinguished from peaks accidentally falling at $\Omega_1 = 0$ either by changing the offset used in the encoding (artifacts will not move) and/or by phase cycling or adding a coherence-selection gradient pulse to the t_1 evolution.
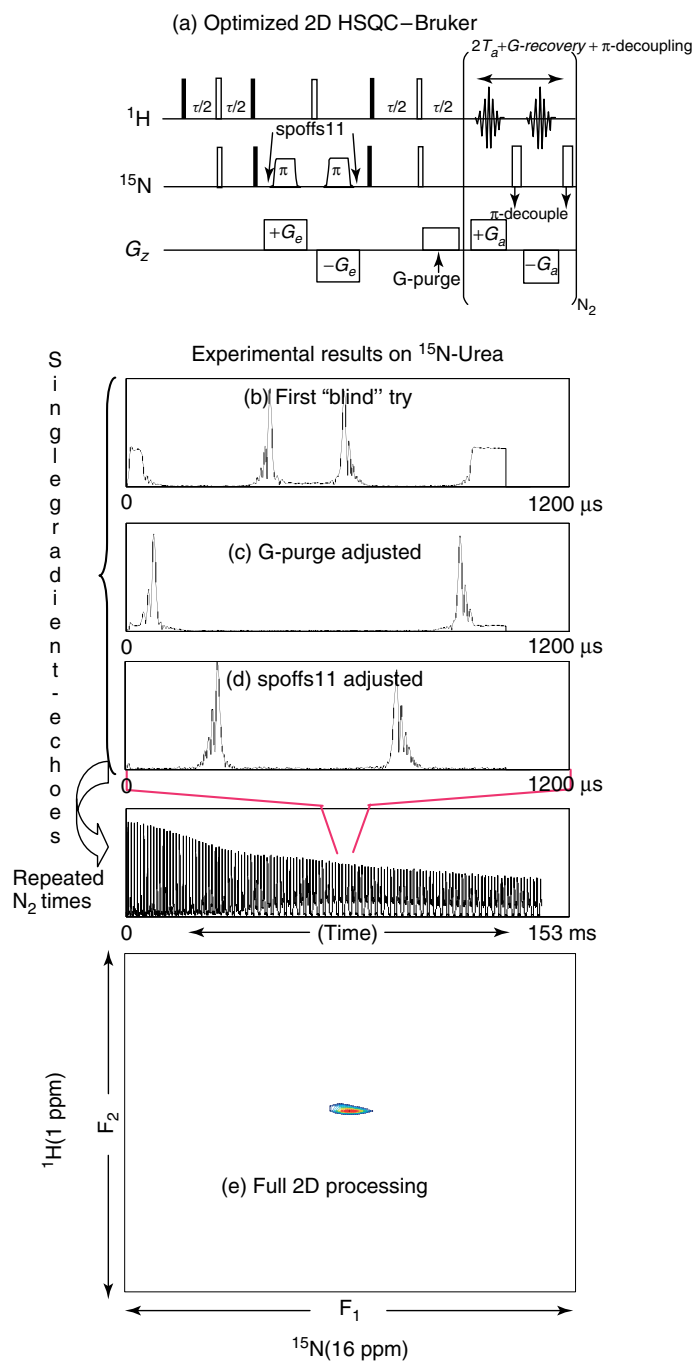
Figure 3.7. As in Figure 3.6, but for the case of constant-time HSQC encoding executed on a Bruker machine. The sample analyzed was ^{15}N-urea, which under the fully decoupled conditions used leads to a single peak in the 2D space. Notice that in this case the presence of heteronuclear decoupling π-pulses inserted in between the G_a gradient recovery times. Thin and thick lines denote nonselective $\pi/2$ and π pulses, respectively.
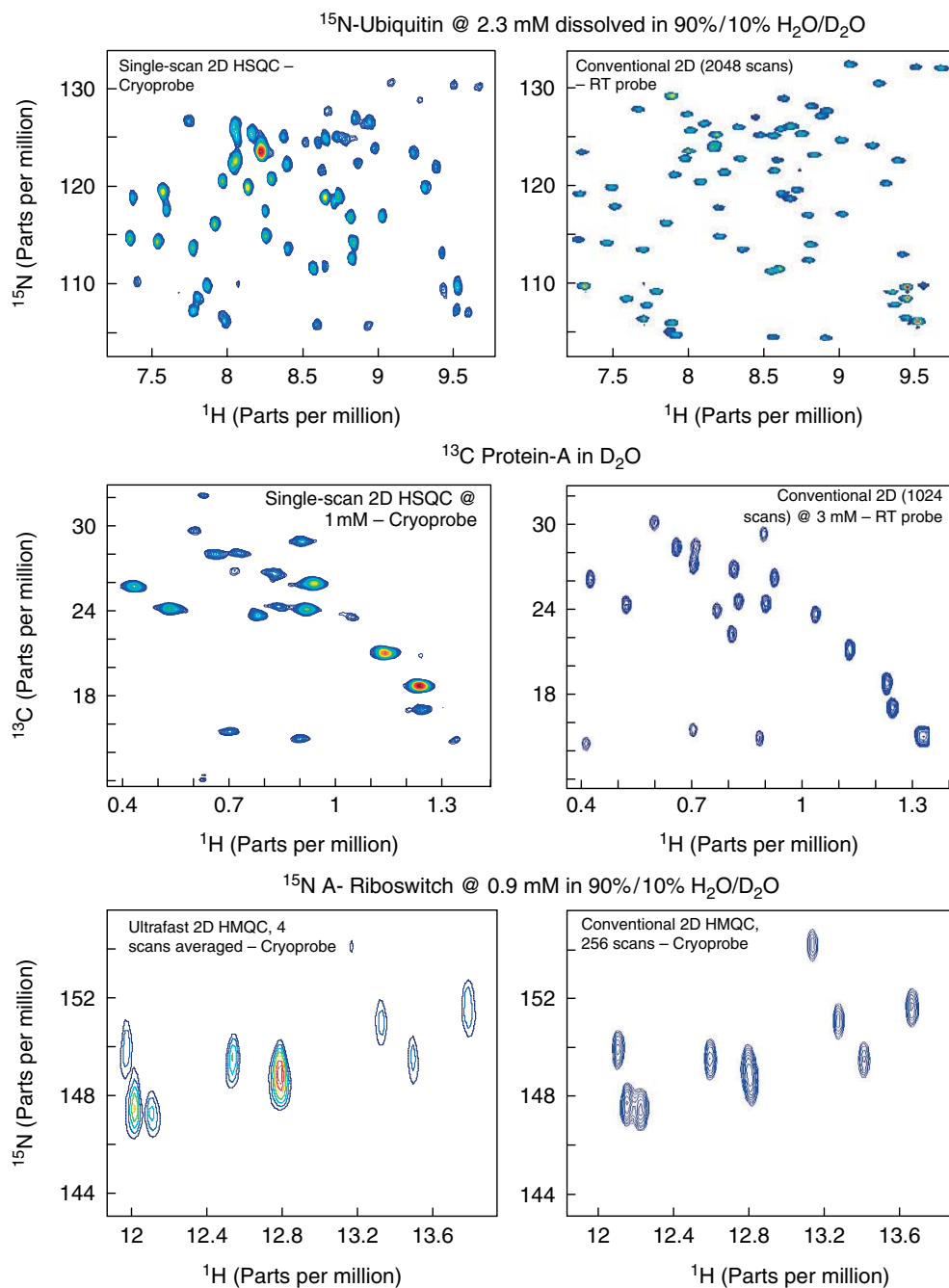
Figure 3.8. An illustration of the performance of ultrafast 2D heteronuclear experiments in biomolecular settings. All data were collected on a Bruker 800 MHz NMR spectrometer under the conditions detailed in the figure, using the principles described in this overview.

earlier will lead from the single-scan FID(t) signal to the full 2D data set being sought (Figure 3.6).

The second sequence that we choose to illustrate is a 2D Heteronuclear Single-Quantum Correlation type experiment, correlating X-nuclei evolution with ^{1}H t_2 detection using a $\pi - \pi$ constant-time spatial encoding combination (Figure 3.7a). The overall idea is as above, and starts by choosing a number of offsets, spectral resolution parameters and windows SW_1, SW_2 that optimize, as far as possible, the encoding and acquisition conditions. On the ^{1}H channel one would then, for instance, use an offset *O1a* to excite the spins and carry out water suppression, but then center the acquisition around the nuclei of interest (e.g., by setting the *O1* on the amide protons) so as to employ the longest T_a possible. Similarly, on the X channel, the offset *O2* of the INEPT modules may differ from the central encoding offset *O2a* (or *spoffs* for the shaped pulse) that positions best the indirect-domain echoes of interest. While most of the considerations involved in setting up these various parameters will remain as in the previous example, a number of differences may arise, including the need for employing larger G_e values so as to compensate for the smaller γ_e of X nuclides, and the need for adding (preferably supercycled) π_X decoupling pulses in between the $\pm G_a$ square-wave oscillation so as to retrieve a fully decoupled F$_2$ trace–with the ensuing time delay becoming part, together with the T_a and the gradient-switching times, of the delays defining Δt_2. Figure 3.7(b–e) illustrates the stages involved in the resulting 2D single-scan acquisition processing, once again using a simple chemical as an example.

3.6 CONCLUSIONS AND PERSPECTIVES

The present summary attempts to give a "hands on" description on how to set up, optimize, and process single-scan 2D NMR experiments, relying on a narrative that we trust will be found pedagogical. Among the various remarks that were made, attention should again be drawn onto SNR, the issue that constitutes the main obstacle standing in front of single-scan 2D experiments–particularly when targeting the analysis of biomolecules in aqueous media, where probe tuning and solvent suppression conditions are usually most challenging. Needless to say the setting up of this kind of experiment, particularly for a first time, can be carried out much

more easily on concentrated samples containing small organic molecules than on dilute systems containing aqueous macromolecular solutions. This does not mean, however, that larger peptides, proteins, and nucleic acids cannot be tackled with these protocols: Figure 3.8 shows a few examples of systems that we have been able to analyze so far with these methods. As can be seen from these traces, relatively high-quality 2D data for proteins and nucleic acids are obtainable by this route, even if still requiring relatively high (1–2 mM) concentrations for retrieving the data in a single scan. Largely responsible for this limitation are the filter bandwidth considerations mentioned in 3.3, constraints that are inherent to the method. Additional SNR degradation problems, however, still stem from nonidealities such as problems with gradient waveforms that broaden the echoes, heteronuclear decoupling complications stemming from gradient-switching times that are too long, and complications in achieving a full suppression of the solvent signal. A further source of peak distortion and SNR loss originates from the difficulties still faced by single-scan 2D NMR encoding schemes in retrieving purely absorptive lineshapes in complex spectra; problems that once again seem associated with the presence of gradient nonidealities. The solution of all these important outstanding aspects will surely involve the combined design of new pulse schemes and of new optimized hardware.

RELATED ARTICLES IN THE ENCYCLOPEDIA OF MAGNETIC RESONANCE

Echo-Planar Imaging

Field Gradients and Their Application

Fourier Transform Spectroscopy

REFERENCES

1. I. J. Lowe, *Phys. Rev. Lett.*, 1959, **2**, 285.

2. R. R. Ernst and W. A. Anderson, *Rev. Sci. Instrum.*, 1966, **37**, 93.

3. R. R. Ernst, G. Bodenhausen, and A. Wokaun, *Principles of Nuclear Magnetic Resonance in One and Two Dimensions*, Clarendon: Oxford, 1987.

4. J. Jeener, in *Ampere International Summer School II*, Basko Polje: Yugoslavia, 1971.

5. W. P. Aue, E. Bartholdi, and R. R. Ernst, *J. Chem. Phys.*, 1976, **64**, 2229.

6. P. Mansfield, *J. Phys. C: Solid State Phys.*, 1977, **10**, 55.

7. P. T. Callaghan, *Principles of Nuclear Magnetic Resonance Microscopy*, Oxford University Press: Oxford, 1991.

8. F. Schmidt, M. K. Stehling, and R. Turner, *Echo Planar Imaging: Theory, Technique and Application*, Springer Verlag: Berlin, 1998.

9. P. Giraudeau and S. Akoka, *J. Magn. Reson.*, 2008, **192**, 151.

10. Y. Shrot and L. Frydman, *J. Chem. Phys.*, 2008, **128**, 164513.

11. L. Frydman, T. Scherf, and A. Lupulescu, *Proc. Natl. Acad. Sci. U.S.A.*, 2002, **99**, 15858.

12. L. Frydman, T. Scherf, and A. Lupulescu, *J. Am. Chem. Soc.*, 2003, **125**, 9204.

13. Y. Shrot and L. Frydman, *J. Am. Chem. Soc.*, 2003, **125**, 11385.

14. L. Frydman, *Compts. Rends. Chimie*, 2006, **9**, 336.

15. Y. Shrot and L. Frydman, *J. Chem. Phys.*, 2008, **128**, 052209.

16. K. Sekihara and H. Kohno, *Magn. Reson. Med.*, 1987, **5**, 485.

17. G. Metzger and X. Hu, *J. Magn. Reson.*, 1997, **125**, 166.

18. M. Mishkovsky and L. Frydman, *J. Magn. Reson.*, 2005, **173**, 344.

19. B. Shapira, A. Lupulescu, Y. Shrot, and L. Frydman, *J. Magn. Reson.*, 2004, **166**, 152.

20. Y. Shrot, B. Shapira, and L. Frydman, *J. Magn. Reson.*, 2004, **171**, 163.

21. B. Shapira, Y. Shrot, and L. Frydman, *J. Magn. Reson.*, 2006, **178**, 33.

22. A. Tal, B. Shapira, and L. Frydman, *J. Magn. Reson.*, 2005, **176**, 107.

23. N. S. Andersen and W. Köckenberger, *Magn. Reson. Chem.*, 2005, **43**, 795.

24. P. Pelupessy, *J. Am. Chem. Soc.*, 2003, **125**, 12345.

25. Y. Shrot and L. Frydman, *J. Chem. Phys.*, 2006, **125**, 204507.

26. P. Giraudeau and S. Akoka, *J. Magn. Reson.*, 2007, **186**, 352.

27. A. Tal and L. Frydman, *J. Magn. Reson.*, 2006, **182**, 179.

28. C. Barratt, E. D. Fackerell, and D. Rosenfeld, *J. Magn. Reson.*, 1989, **85**, 35.

29. Ē. Kupče and R. Freeman, *J. Magn. Reson. A*, 1996, **118**, 299.